Plasma spraying of mullite and pore formers for thermal insulating applications

Vincent Fournier, Aurélie Quet, Erick Meillot, Hélène Ageorges

Plasma spraying of mullite and pore formers for thermal insulating applications

Vincent Fournier[1,2] (vincent.fournier@cea.fr), Aurélie Quet[1] (aurelie.quet@cea.fr), Erick Meillot[1] (erick.meillot@cea.fr), Hélène Ageorges[2] (helene.ageorges@unilim.fr),

[1]CEA, DAM, Le Ripault, F-37260 Monts, France

[2]Université de Limoges, IRCER, 87068, Limoges, France

Abstract

Porous materials are widely used in various fields requiring thermal insulation properties, such as the aircraft industry, with thermal barrier coatings. In such applications, plasma-sprayed yttria-stabilized zirconia proved to be a highly effective insulating coating. With higher void content, materials such as aluminum silicate are used in space industry (Intermediate eXperimental Vehicle, for instance) due to their low density and thermal conductivity.

In this study, several thermal sprayed coatings were evaluated as candidates for low thermal conductivity applications. Porous deposits were produced thanks to the pore former introduction into the plasma plume, and so integrated inside coatings. Two pore formers were used, aromatic polyester and a mineral agent, leading to different microstructures. Porous mullite microstructures, with 80 % porosity due to polyester removal by thermal treatment, were carried out, while layered microstructures were obtained with the mineral agent and low enthalpy plasma. Furthermore, thick coatings were sprayed with different plasma spraying configurations. A static spray set-up allowed porous one centimeter thick coating production without any manufacturing defects before and after thermal treatment. This was made possible throughout a deposit temperature control, via a cryogenic carbon dioxide cooling system.

Keywords: Porous ceramic materials, Atmospheric plasma spraying, Pore formers, Thick coatings

1. Introduction

A porous ceramic can be defined as a material having a total void content between 20 and 95%. Porous ceramics are composed of two distinct phases, a solid phase or skeleton ceramic and a gaseous phase which is usually air inside pores.

Nowadays, porous ceramics are subject to a huge attention in the industry field, they are used in several thermal insulation related applications, carriers for catalysts [1], filters [1], bone substitutes [2], [3], lightweight structure components. In broad terms, porous ceramic materials have great thermal shock resistance abilities, a high chemical stability and an excellent abrasion resistance. Moreover, properties such as low thermal conductivity, low density, and high temperature resistance, make them prime candidates for insulating applications. In most cases, control of pore characteristics is a key element to manage their fabrications. Indeed, parameters such as pore shape or size distribution directly impact thermal and mechanical properties of manufactured materials, and thus their applications.

To realize such porous ceramic materials, several manufacturing methods exist, like direct foaming method [4], replica technique and sacrificial template method. Depending on target application and method, it is possible to cover overall porosity characterized by an average pore size from 0.4 to 4 mm [4]. For most porous materials, porosity, up to 90 %, is open type: pores are connected to each other with a more or less developed network according to the used process, which manages the pore size distribution.

In this work, air plasma spraying process was studied to achieve porous ceramic coatings for insulating applications, such as in the Intermediate eXperimental Vehicle (IXV [5]). This process has the distinctive feature of manufacturing coatings with particular geometries at low cost. To the best of our knowledge, ceramic sprayed coatings with porosity rates higher than 50 % were never reported in the present literature. Conventionally in the plasma spraying field, porosity rates are between 10 and 30 %, restraining the use of coatings

in applications described above. At best, 40 to 45 % porosity were reached in Thermal Barrier Coatings (TBCs) applications [6], [7], [8], [9], [10], [11] or others applications. For instance, Ctibor et al. [12] developed porous tourmaline deposits (44 % of porosity). An already described approach involves the use of pore formers. Spraying pore former with ceramic powder leads to porous ceramic coatings, once foaming agent removed. By controlling pore former size, morphology, nature and treatment, different architectures and microstructures can be obtained. A wide variety of sacrificial materials were used as pore formers: salts (sodium chloride [2], [13], [14], [15], [16], sodium fluoride [17]), natural and synthetic organics (poppy seed [18], wheat particles [19], carbamide [20], [21]), metals and ceramic compounds (zinc oxide [22], nickel [23]) and polymers (PMMA [24], polyester [25], polystyrene [26], [27], [28]).

Requirements enforce low thermal conductivity and density, which limits the choice to aluminum silicates, such as mullite which is commonly used in plasma spraying [29], [30], [31], [32]. Mullite (stoichiometry: 3 Al_2O_3 – 2 SiO_2) is an advanced ceramic having appropriate properties for thermal insulating applications, such as compressive strength, thermal conductivity [33], corrosion resistance [34] and stability in atmospheric pressure [35], [36]. The mullite main properties obtained with the CES (Cambridge Engineering Selector) software are represented in Table 1.

This work explored the possibility to manufacture thick porous mullite coatings by using an air plasma spraying process with two different pore formers: an organic one (aromatic polyester already employed in the present literature for TBCs applications) and a mineral agent.

The first part of this article was dedicated to the architectural development of free standing porous mullite coating obtained with one millimeter thickness. Then, the work consisted in produce free standing porous mullite coatings, with one centimeter thickness.

Three plasma spraying configurations were considered to achieve thick deposits. The first one carried out a cylindrical configuration, which is the spray set-up used for the architectural development. The second was the planar configuration and the last one, the static configuration.

2. Experimental procedure

2.1. Feedstock powders

In order to get different porosity networks two different mullite powders were used, Fig. 1:

- A fused and crushed mullite powder (Oerlikon Metco, Switzerland) with a size distribution of -42+5 µm (Fig. 1a);
- An agglomerated and sintered mullite powder (Höganäs, Sweden) with a size distribution of -79+37 µm (Fig. 1b);

Between 5 and 40 % porosity can be easily obtained by plasma spraying process with appropriate powder and plasma parameters. In consequence, two pore formers were used to exceed this value, polyester and a mineral agent:

- Aromatic polyester powder (Oerlikon Metco, Switzerland) does not show any melting temperature but a decomposition temperature and has a size distribution of -84+44 µm with cauliflower type topography used as pore former. It will be called organic pore former or polyester in what follows (Fig. 1c);
- The mineral agent shows a melting temperature and gives, after elimination, a lamellar porosity. As CEA developed the know-how of this sprayed material, its properties and nature will not be discussed in this work.

2.2. Plasma co-spraying process

All feedstock were sprayed by an atmospheric plasma spraying system (Fig. 2), equipped with a F4-MB torch (Oerlikon Metco, Switzerland), fixed on a 6-axis robot.

For architectural development of porous materials, mullite coatings with high overall porosity were deposited on aluminum substrates (50x50x2 mm) with one millimeter thickness. A second set of larger substrates was also used (100x100x5 mm) in order to analyse scale troubles in larger deposition of mullite coatings with one centimeter thickness. These plates are intended to be used for thermal experiments in order to quantify their insulation power. In all cases, coatings were removed from substrates for porosity measurements. This was made possible by spraying a mineral or organic bond coat eliminated once spraying is over. This approach will be discussed in the results part. Before spraying, each substrate was grit-blasted by alumina abrasive powder to enhance the surface roughness (about 4.5 µm) in order to guarantee the mechanical interlocking between coating and substrate. Substrates were beforehand degreased with ethanol and mounted on a cylindrical fixture rotating around a vertical axis in front of the plasma torch as illustrated in Fig. 2. During spraying, the torch moved along this vertical axis with a speed movement at 12 mm/s and a fixed standoff distance (110 mm). The cylinder had a uniform rotation of 119 rpm that corresponds to a step size of 6 mm and a linear speed of 1,000 mm/s (relative torch/substrate velocity). The velocity control warranted homogenous thicknesses on substrates. Moreover, a cryogenic cooling system was placed on the plasma torch to maintain a surface temperature around 50 °C. This temperature was measured with an embarked pyrometer placed on the 6-axis robot. The cryogenic system could increase molten particles quenching rate and could affect coating crystallinity and adhesion [37], [38].

A co-spraying method, as illustrated in Fig. 2b, was used allowing two different powder injections: the aluminium silicate powder injector was positioned at 6 mm from the torch nozzle exit and 7 mm from the torch axis while the pore former injector was downstream (see position explanation below). In co-spraying, one plasma parameter set is

used to treat several materials. In this study, plasma conditions were chosen for an ideal thermal treatment of aluminum silicates. That is why, injection characteristics of pore forming agents were changed (injection distance from the anode surface for example). Pore formers were injected downstream into the plasma plume, compared to the ceramic injection. These distances varied depending on the pore former nature and spraying parameters. The organic pore former injection distance was 18 and 40 mm, for conditions A and C, respectively. For the mineral agent, these distances were 25 and 35 mm for plasma parameters A and C, respectively. The argon gas carrier rate was also modified in order to systematically have a powder deviation angle of 3-4°, which allowed an ideal thermal treatment of sprayed powders [39].

The plasma conditions A and C are summarized in Table 2. These conditions were chosen in order to observe notable differences in as-sprayed coating microstructures due to plasma temperature and velocity. From condition A to C, succinctly, electric intensity and dihydrogen rate increased. In plasma spraying field, it is well known that velocity depends mainly on the square root of intensity for ternary plasma [40], [41]. So, an increase in intensity leads to an increase in plasma and particles velocity [42], [39]. Regarding the dihydrogen rate increase, it enhances plasma thermal conductivity which leads to an increase of plasma enthalpy. So, from plasma parameter set A to C, an increase of plasma velocity and temperature is observed.

Manufacturing thick porous mullite coatings implied investigations of different spray set-up and substrates. These points will be discussed in the result part.

2.3. Microstructural analysis

In order to observe coating microstructure, samples were mounted in epoxy resin, before cross-section polishing. The samples surface was sandpapered with silicon carbide polishing papers (P320, P800, P1200, P2000 and P4000), before polishing with a diamond

suspension of 1 µm with a Struers polisher (Tegra Pol 21). Then, samples were washed and dried by alcohol. All the observations were performed using an Olympus microscope (BX 60 M) and a Phenom Pure SEM in BSD mode. In all cases, the bond coat, and so the substrate, were removed for porosity measurements. The overall porosity rates were measured on SEM micrographs using a low magnification (x500). In these pictures, the black phase refers to the porosity while the grey/white ones were linked to mullite. Porosity rates were determined by using the ImageJ software. This software allows enhancing the contrast and luminosity of SEM images; porosity rate was evaluated after threshold step.

3. Results and discussions

3.1. Plasma co-spraying of mullite and pore formers

Fig. 3 represents polished cross-section (Fig. 3a,b,c) and fracture surface (Fig. 3d,e,f) for three different mullite microstructures sprayed with co-spraying plasma process. The first microstructure (Fig. 3a) was obtained with the aromatic polyester pore former with the plasma condition C while others were performed with the mineral agent, with different feed rate powders, particle size distributions and plasma spraying conditions. It should be noted that all these microstructures were strongly different, resulting from two main strategies.

3.1.1. First strategy

The first strategy concerns microstructures represented in Fig. 3a,c,d,f. The idea was to obtain a thin and homogenous ceramic spatial distribution inside the coating after pore former removal. To achieve that, it was essential to spray powder with a narrow particle size distribution and suitable powder morphology to lead to a good particle thermal treatment by the plasma plume. In that case, the fused and crushed morphology was more adapted than the agglomerated and sintered form; the particle size distribution was also narrower. Besides, creating the homogeneous ceramic network required to increase as much as possible the flattening degree of droplets impacting the substrate and underlying splats. In consequence, it

was crucial to increase plasma velocity, hence the use of plasma parameter set C. Mullite particles, thanks to their higher kinetic energy, will impact the substrate and spread over it [39], leading to a splashing phenomenon. This phenomenon was intensified with an increase in particle melting degree, due to a dihydrogen rate increase. As a result, this strategy was appropriate to elaborate porous microstructures with overall porosity rates from 75 to 80 % according to the pore former nature.

A thermal treatment was essential to remove the organic pore former and obtain the porous ceramic skeleton. This treatment was performed at 500 °C during 4 hours in an oven under air. Some TGA/DSC experiments were done in order to assure that all the aromatic polyester was removed: these results are shown in Fig. 4. The whole polyester burnt at temperatures around 550 °C, but its thermal decomposition begins around 350 °C. Accordingly, a 500 °C thermal treatment was sufficient to evacuate entirely the aromatic polyester in one millimeter thick coating. A porous mullite coating with a porosity rate close to 80 % was obtained after thermal treatment (Fig. 3a). The coating microstructure was mainly composed of spherical open porosity due to the pore former nature.

The mineral pore former evacuation will not be discussed in this work. However, it can be said that the mineral agent used as pore former presents a melting point which is not physically the case for the aromatic polyester. This melting temperature was responsible for observed differences between microstructures represented Fig. 3a,c,d,f. Indeed, using the same fused and crushed mullite powder, microstructures obtained with the mineral agent were more lamellar, which leads mainly to the establishment of lamellar open porosity. This kind of microstructure explained the porosity rate decrease measured thanks to the ImageJ software, compared to the porous microstructure obtained with the aromatic polyester removal.

To conclude with this strategy, the polyester nature lets its footprint in the deposit. Indeed, through Fig. 3a,d, the pore morphology is spherical as the initial polyester morphology. So, the initial morphology was maintained after spraying. In this way, coating build-up consists of stacking both polyester particles and mullite droplets with a high kinetic energy in order to introduce the splashing phenomenon. Through Fig. 3c,f, the pore morphology was more disordered, the initial pore former powder morphology was not maintained, and the coating was more heterogeneous and brittle due to the lamellar aspect.

3.1.2. Second strategy

The second strategy was dedicated to the manufacturing of a completely different microstructure than those presented above, by using:

- The mineral pore former, which has physically a melting temperature;
- The plasma parameter set A, which was completely the opposite of the parameter set C in terms of plasma velocity and temperature in order to build large ceramic splats.

Consequently, the microstructure morphology and its architecture were completely different from those previously observed.

So, layered microstructures were obtained with the widest particle size mullite powder (Fig. 3b,e). In these microstructures, the stratum number corresponds to the pass number referred by 6-axis robot in front of the substrate. Contrary to the microstructures resulting from the polyester removal, this kind of layered microstructures was not suitable for coating mechanical cohesion. In consequence, overall porosity rates do not exceed approximatively 65 %. However, for thermal insulating applications, these layers were very promising. Thermal transfer inside coating thickness and overall thermal conductivity are drastically reduced.

To conclude with the architectural development, one set of porous deposits, obtained using the aromatic polyester, presents a chaotic and disordered microstructure with porosity rates up to 80 %. Another set of coatings was performed with a mineral pore former resulting in layered microstructures and overall porosity rates between 65 and 75 %, depending on plasma parameters and initial starting powder. In all cases, the overall porosity is an open porosity induced by the pore former removal; the closed porosity does not exceed 4 % in any ceramic porous microstructure.

Based on these architectural approaches, the development of as-sprayed coatings with one centimeter thickness were considered.

3.2. Thick porous mullite coatings

3.2.1. Cylindrical configuration

Requirements mention porous coatings with one centimeter thickness for thermal insulating applications. It was decided, in a first step, to realize these coatings with the spray set-up described in Fig. 2 (plasma co-spraying process used for the architectural development of porous mullite deposits) and to use the aromatic polyester described Fig. 1c to generate all thick porous mullite coatings. Spraying one millimeter samples, as presented above, was realized experimentally by controlling the cryogenic cooling system used. The main differences in order to build thick coatings lie in the feed powder rates. Indeed, it is necessary to take into consideration the deposition efficiency, and not only the thermal efficiency, defined by the deposited thickness in one spray cycle. In the cylindrical configuration case, one cycle refers to two passes, back and forth of the plasma torch. To reduce as much as possible the plasma spraying duration, it is useful to work with high efficiencies. Indeed, long spraying duration increases the risk of manufacturing defect appearance. These manufacturing defects could be a problem in the powder flowability: an injector clogging phenomenon can easily appear in the co-spraying process, when several injectors are used. In fact, some very

fine powders were not fully treated by the plasma jet and so scattered in all directions. In some cases, and for long spraying duration, these partially melted droplets reach the upstream injector. This can influence the powder flow into the plasma plume and so the spraying efficiency.

In this study, some mullite powders can be located on the aromatic polyester injector. That is why, in all cases, the distance between the foaming agent injector and the torch axis was different, compared to the ceramic injector, as illustrated Fig. 2. One last defect can appear, linked to the cryogenic liquid carbon dioxide cooling system. Depending on the outside atmosphere, meteorological conditions and spraying durations, some humidity can disturb the carbon dioxide cooling of coatings during spraying and so affect surface temperature.

A first step was to realize a thick porous mullite microstructure with 70 % porosity rate to avoid mechanical debonding or deterioration problems. Word “thick”, in following sections of this document, will always refers to one centimeter thickness.

With the cylindrical configuration introduced previously, a thick sample was obtained, as illustrated in Fig. 5a; its microstructure is represented Fig. 5b. Compared to the spraying of porous coatings above (Fig. 3a), heat treatments were performed at 900 °C during 1 h on deposits to be sure that the organic pore former is entirely removed inside thick mullite coatings. As a result, samples were perfectly flat without visible manufacturing defects after spraying and treatment. There was no shrinkage phenomenon during the oven treatment. These coatings were free standing thanks to an initial mineral bond coat sprayed on aluminum substrates to allow coatings removal after spraying and before thermal treatment. The deposition efficiency associated to the plasma parameter used was around 70 µm by cycle. As a result, one centimeter thickness required 150 cycles. In order to take a look at coatings, especially on the deposition efficiency which can vary with the thickness, to prevent eventual

manufacturing defects at coating surface, but also to keep the standoff distance constant during the coating build-up, the spraying was divided into three sequences.

So, free standing mullite samples with an overall porosity rate of 70 % were obtained by controlling the cryogenic cooling system, thus temperature surface and by adjusting feed rate powders. In order to upgrade the coating build-up scale, the aluminum substrate size was changed from 50x50x2 mm to 100x100x5 mm. In consequence, spray set-up had to be changed too.

3.2.2. Planar configuration

Larger plate dimensions were not consistent with the cylinder size. So, a new configuration, called as planar configuration or planar spray set-up, was defined (Fig. 6). This implied to modify both the robot kinematic and cryogenic system parameters. In this configuration, the device rotation speed is variable as well as the torch movement speed in order to keep constant the linear speed (1,000 mm/s). However, the experimental strategy and spraying efficiencies were identical. Aluminum substrates stand close to the support centre where the rotation speed is higher to decrease spraying duration and the manufacturing defect appearance risk. As a result, same microstructures than those already presented Fig. 5b were obtained, that is to say, a microstructure with 70 % of porosity and an apparent density of 0.85. However, it was not possible to build thick coatings. When the coating thickness reached approximatively 3 mm, a delamination phenomenon occured. The coating and mineral bond coat spontaneously peeled off during spraying. In order to prevent this phenomenon, the mineral bond coat thickness was decreased from 200 to 100 µm and the surface roughness was increased from 4.5 to 9.0 µm: coating only thickened from 3 to 4 mm (Fig. 7). Because of the poor adhesion of the mineral agent on aluminum substrates during spraying, it was not possible at first glance with this set-up to build coatings at the centimeter scale. So, it was decided to change the bond coat nature from mineral to organic one. As a

consequence, the substrate nature changed too. Obtaining free standing samples after plasma spraying requires a thermal treatment for organic pore former removal. So, stainless steel was used as substrate, the experimental approach summary is detailed Fig. 8. The surface roughness for stainless steel substrates was about 6.5 - 7.0 µm and the organic bond coat thickness around 130 µm.

In order to illustrate the poor adhesion of the mineral agent as bond coat, the In-Situ Coating Property (ICP-8) Sensor was used (Fig. 9a). It is a commercial device provided by Reliacoat Technologies which allows calculating residual stresses inside standardised samples. This device was used in the case of thick coating spraying to illustrate the delamination phenomenon and not to quantify the quenching stresses generated by plasma spraying process. A slight modification was made with the ICP Sensor. Indeed, in order to not restrain the coating to the substrate during its manufacturing, projection masks were placed in front of fixation screws (Fig. 9a **(3)**). Two experiments were made with this device on aluminum substrates: one spraying of mullite/polyester was made on mineral bond coat and another was made on organic bond coat. The obtained samples are represented in Fig. 9b: **(4)** represents the sample obtained with a mineral bond coat while **(5)** represents the sample obtained with the organic bond coat. A partial delamination can be observed with the mineral bond coat once the thickness coating reaches 5 mm. For the organic bond coat, it was possible with the same spray set-up to build a 7.5 mm coating thickness without any visible manufacturing defects. By modifying the substrate surface roughness and bond coat thickness, it was not possible to build this thickness when the mineral agent is employed as bond coat. These results were only applicable with the used standard samples (22.9x2.5x2.3 mm) and the used configuration. Indeed, in the planar configuration case and plate utilization as substrate of dimension 100x100x5 mm, the delamination phenomenon occurred before the coating thickness reaches 4 mm. These different coating thicknesses can be explained by the used

configuration and by surface temperature. So, quenching stresses were higher in the case of the planar configuration compared to the ICP configuration, this was explained in Fig. 13.

With the use of the organic agent as bond coat, large and thick mullite plates (100x100x10 mm) with 70 % porosity were obtained (Fig. 10). They presented no surface defects, no shrinkage phenomenon during spraying or thermal treatments. Two different thermal treatments were achieved. One treatment at 500 °C during 4 hours to remove the organic bond coat (slope of 5 °C/min). Another treatment at 900 °C, during 1 hour, to remove all the polyester inside the coating (slope of 5 °C/min).

By changing the bond coat nature, a thick coating was obtained, which was not possible with the mineral bond coat, even by playing with the roughness surface and bond coat thickness.

However, a new problem appeared: free standing thick coatings present all an asymmetrical curvature before and after the thermal treatment at 900 °C during 1 hour, after the entire organic pore former removal. Furthermore, a deformation at all plate edges appears during plasma spraying, especially for the two plate edges located close to the support centre where plate rotation speed is higher. At these locations, surface temperature is also higher than the one in the other parts of plates leading to an inhomogeneous surface temperature during spraying. At first glance, this curvature phenomenon was attributed to surface temperature and residual stresses induced during spraying process by the droplets spreading and their solidification with an extremely high quenching rate. This quench is intensified with the carbon dioxide cryogenic cooling. The curvature problem will be detailed in the following subsection. In order to keep better track of spraying temperature, a third configuration called as static configuration or static spray set-up, was studied (Fig. 11). In this configuration, the spraying support is fixed.

3.2.3. Static configuration

Robot kinematic changed again, as well as the cryogenic system parameters. In this spray set-up, the plasma torch had a traverse speed of 1,000 mm/s. One cycle corresponded to one pass; the spray pattern and set-up are presented Fig. 11. Thick porous mullite coatings with an overall porosity of 70 % and an apparent density of 0.85 were obtained, as showed in Fig. 12. There was no more curvature problems related to temperature elevation during spraying. In this way, coatings were sprayed with a deposition efficiency of 35 µm by cycle, requiring 300 cycles to obtain one centimeter thick deposits. Plasma spraying duration was divided into two parts of 45 min, each pass lasted around 20 s. Regarding the organic bond coat, its thickness was always equal to 130 µm and surface roughness of substrates did not changed between previous configurations. In that case, the curvature problem was solved by changing the spraying configuration.

Fig. 13 presents the surface temperature evolution depending on the spray set-up. As said before, this temperature was measured with a robot-embarked pyrometer. Both spray pattern used were also represented. In the planar configuration, surface temperature was not homogeneous and varied between 30 and 140 °C, depending on the plasma plume location on the spraying support. When the plasma torch moved away from this centre, in location 1, temperature was between 30 and 50 °C. Close to the spraying support centre, in location 2, temperature exceeded 130 °C. With homogeneous coating surface cooling during global spraying, differences in measured temperatures were observed. Plate edges located close to the spraying support centre were lightly peeled off during spraying. This phenomenon was due to the rotation speed increase when the plasma torch moved to the spraying support centre. It was also due to the heat evacuation issue from plasma plume and droplet impact. This phenomenon could be reduced by increasing the cooling at location 2 (Fig. 13a), without interfering with the temperature measurements at location 1. This was not possible because of the cooling inertia and spraying duration: one pass lasted around 15 s.

In the static configuration, spraying support and so substrate did not moved, and so surface temperatures oscillated between 30 and 80 °C and seemed to be more homogeneous during spraying. No manufacturing defects or edges peeled off were experimentally found on mullite/polyester coatings before heat treatment.

Curvature problem can be linked to residual stresses, particularly to quenching stresses because of the lightly delamination occurring during spraying. This also means that the coating is in a tensile state during its build-up. On one hand, an increase in quenching stress appears with deposit temperature. Indeed, quality of the interlamellar contact, both mechanical and thermal, improves when the piece superficial temperature increases. On a second hand, as reported many times in literatures, quenching stresses increase with a coating thickness increase as well as thermal stresses. However, depending on the material nature and deposit temperature, relaxation of quenching stresses inside the coating thickness can appeared [43]. In most cases, these relaxations lead to cracks inside splats at the microscopic scale, and inside the entire coating at macroscopic scale [44].

In future work, quenching and thermal stresses of mullite coatings sprayed with all kind of pore formers will be estimated by curvature measurements. The ICP Sensor [45] introduced previously will be used to quantify stresses induced by materials during plasma spraying in order to corroborate residual stresses evolution obtained in the present literature in the case of high thick coating build-up [44].

4. Conclusions

In this work, mullite porous coatings were built-up by an atmospheric plasma co-spraying process using two kinds of mullite raw powders: a fused and crushed one with a size distribution of -42+5 µm and an agglomerated and sintered one of -79+37 µm. Porosity was obtained thanks to the introduction of pore formers in the plasma plume and so integrated inside the coatings. By eliminating the pore former, a porous ceramic skeleton is obtained.

Besides, playing on the pore former nature, different microstructures with different pore size distributions were performed:

- Porous deposits obtained using an aromatic polyester pore former present a chaotic and disordered microstructure with porosity up to 80 %. This deposit was obtained with a narrow particle size distribution, a fused and crushed powder and a high enthalpy plasma;
- A second layered microstructure was generated with porosity values close to 66 % using a mineral pore former. This microstructure was obtained with a low enthalpy plasma and an agglomerated and sintered morphology powder. Due to layered phenomenon, porosity rates and mechanical cohesion are lower than the previous microstructure;
- A third coating with an intermediary overall porosity, up to 75 %, was obtained after the mineral agent removal, with the fused and crushed powder. This microstructure has lamellar type porosity suitable to decrease the apparent thermal conductivity. However, this kind of porosity induces low mechanical cohesion, compared to the first microstructure.

Furthermore, one centimeter thick coatings were obtained, thanks to the understanding of the cryogenic cooling system, residual stresses evolution and plasma spray set-up kinetic. Thick mullite/polyester coatings were sprayed on aluminum substrates of dimensions 50x50x2 mm. By changing substrate nature, plasma spraying configuration and bond coat nature, plates of mullite/polyester of dimensions 100x100x10 mm were obtained. The poor adhesion when using a mineral agent as bond coat was illustrated by the ICP Sensor. However, even by considering all these changes, plate edges were slightly peeled off during plasma spraying, this was attributed to surface temperature which reaches almost 150 °C, and thus to quenching stresses induced during spraying. Thanks to the static plasma spraying configuration, these phenomena were reduced as much as possible and planar

mullite/polyester plates were obtained. Final heat treatments led to thick porous mullite plates of dimension 100x100x10 mm. These porous mullite plates will be used for thermal experiments.

Residual stresses measurements would be undertaken to quantify, inter alia, the influence of the cooling cryogenic system during plasma co-spraying (matrix and pore former), in order to corroborate what was realized experimentally with thick plate spraying.

References

[1] T. Konegger, R. Patidar, R.K. Bordia, (2015), A novel processing approach for free-standing porous non-oxide ceramic supports from polycarbosilane precursors, J. Eur. Ceram. Soc. 35:2679-2683.

[2] L. Wei, X. Zhang, L. Geng, (2019), Microstructure and properties of NiTi foams with 69 % porosity, Vacuum 162:15-19.

[3] T. Aydoğmuş, Ş. Bor, (2009), Processing of porous TiNi alloy using magnesium as space holder, J. Alloy. Compd. 478:705-710.

[4] A.R. Studart, U.T. Gonzenbach, E. Tervoort, L.J. Gauckler, (2006), Processing routes to macroporous ceramics: A review, J. Am Ceram. Soc. 89(6):1771-1789.

[5] S. Dutheil, J. Pibarot, D. Tran, J.-J. Vallee, J.-P. Tribot, (2016), Intermediate experimental vehicle, ESA program aerodynamics-aerothermodynamics key technologies for spacecraft design and successful flight, Acta Astronautica 124:31-38

[6] K. Bobzin, L. Zhao, M. Öte, T. Königstein, (2019), A highly porous thermal barrier coating based on Gd_2O_3-Y_2O_3 co-doped YSZ, Surf. Coat. Technol. 366:349-354.

[7] S. Siegmann, N. Margadant, L. Zysset, A. Zagorski, M.Arana-Antelo, (2003), Influence of particles velocity and temperature on the properties of thermally sprayed coatings, Proceedings of Les Premières Rencontres Internationales sur la Projection Thermique, Lille, 66-76.

[8] Y. Zhao, J. Wen, F. Peyraut, M.-.P. Planche, S. Misra, B. Lenoir, J. Ilavsky, H. Liao, G. Montavon, (2020), Porous architecture and thermal properties of thermal barrier coatings deposited by suspension plasma spray, Surf. Coat. Technol. 386.

[9] W.-W. Zhang, G.-R. Li, Q. Zhang, G.-J Yang, (2017), Multiscale pores in TBCs for lower thermal conductivity, J. Therm. Spray. Technol. 26(5):1183-1197.

[10] M. Arai, H. Ochiai, T. Suidzu, (2016), A novel low-thermal-conductivity plasma-sprayed thermal barrier coating controlled by large pores, Surf. Coat. Technol. 285:120-127.

[11] D. Aussavy, R. Bolot, G. Montavon, F. Peyraut, G. Szyndelman, J.Gurt-Santanach, S. Selezneff, (2016), YSZ-Polyester abradable coatings manufactured by APS, J. Therm. Spray. Technol. 25(1-2):252-263.

[12] P. Ctibor, B. Nevrlá, Z. Pala, L. Vrtiška, (2018), Natural tourmaline as an efficient alternative to ceramic-type material for plasma spraying, J. S. Afr. I. Min. Metall. 118(4):387-393.

[13] B. Ye, D.C. Dunand, (2010), Titanium foams produced by solid-state replication of NaCl powders, Mater. Sci. Eng. A 528:691-697.

[14] A. Bansiddhi, D.C. Dunand, (2008), Shape-memory NiTi foams produced by replication of NaCl space-holders, Acta Biomater 4:1996-2007.

[15] M. Hakamada, T. Kuromura, Y. Chen, H. Kusuda, M. Mabuchi, (2006), Sound absorption characteristics of porous aluminum fabricated by spacer method, J. Appl. Phys. 100:114908-1 114908-5.

[16] T. J. Fitzgerald, V.J. Michaud, A. Mortensen, (1995), Processing of microcellular SiC foams, Part II, Ceramic foam production, J. Mater. Sci. 30:1037-1045.

[17] A. Bansiddhi, D.C. Dunand, (2007), Shape-memory NiTi foams produced by solid-state replication with NaF, Intermetallics 15:1612-1622.

[18] E. Gregorová, W. Pabst, (2007), Porous ceramics prepared using, poppy seed as a pore-forming agent, Ceram. Int. 33:1385-1388.

[19] K. Prabhakaran, A. Melkeri, N.M. Gokhale, S.C. Sharma, (2007), Preparation of microporous alumina ceramics using wheat particles as gelling and pore forming agent, Ceram. Int. 33:77-81.

[20] O. Smorygo, A. Marukovich, V. Mikutski, A.A. Gokhale, G.J. Reddy, J.V. Kumar, (2012), High-porosity titanium foams by powder coated space holder compaction method, Mater. 83:17-19.

[21] B. Jiang, N.Q. Zhao, C.S. Shi, X.W. Du, J.J Li, H.C. Man, (2005), A novel method for making open cell aluminum foams by powder sintering process, Mater. 59:3333-3336.

[22] M. Rajamathi, S. Thimmaiah, P.E.D. Morgan, R. Seshadri, (2001), Macroporous materials from crystalline single-source precursors through decomposition followed by selective leaching, J. Mater. Chem. 11:2489-2492.

[23] H. Kim, C. da Rosa, M. Boaro, J.M. Vohs, R.J. Gorte, (2002), Fabrication of highly porous yttria-stabilized zirconia by acid leaching nickel from a nickel-yttria-stabilized cermet, J. Am. Ceram. Soc. 85(6):1473-1476.

[24] A.K. Gain, H.-Y. Song, B.-T. Lee, (2006), Microstructure and mechanical properties of porous yttria stabilized zirconia ceramic using poly methyl methacrylate powder, Scr. Mater. 54:2081-2085.

[25] M. Arai, T. Suidzu, (2012), Porous ceramic coating for transpiration cooling of gas turbine blade, J. Therm. Spray Technol. 22(5):690-698.

[26] A. Ramezani, S. Nemat, S.M. Emami, (2018), Effects of the size of expanded polystyrene as a pore-former on the properties of insulating firebricks, Ceram. Int. 44:6641-6644.

[27] Y. Hotta, P.C.A. Alberius, L. Bergström, (2003), Coated polystyrene particles as templates for ordered macroporous silica structures with controlled wall thickness, J. Matter. Chem. 13:496-501.

[28] E.G. de Moraes, M. Bigi, N.P. Stochero, S. Arcaro, C. Siligardi, A.P. Novaes de Oliveira (2019), Vitrocrystalline foams produced with EPS as pore former: Processing and characterization, Process. Saf. Environ. 121:12-19.

[29] S. Li, X. Xi, G. Hou, Y. An, X. Zhao, H. Zhou, (2015), Preparation of plasma sprayed mullite coating on stainless steel substrate and investigation of its environmental dependence of friction and wear behavior, Tribol. Int. 91:32-39.

[30] G. Di Girolamo, C. Blasi, L. Pilloni, M. Schioppa, (2010), Microstructural and thermal properties of plasma sprayed mullite coatings, Ceram. Int. 36:1389-1395.

[31] S. Li, X. Zhao, G. Hou, W. Deng, Y. An, (2016), Thermomechanical properties and thermal cycle resistance of plasma sprayed mullite coating and mullite/zirconia composite coatings, Ceram. Int. 42:17447-17455.

[32] Y. Wang, R.S. Lima, C. Moreau, E. Garcia, J. Guimaraes, P. Miranzo, M.I. Osendi, (2009), Mullite coatings produced by APS and SPS: Effect of powder morphology and spray processing on the microstructure, crystallinity and mechanical properties, proceeding of the 2009 International Thermal Spray Conference and Exposition, p. 97.

[33] P. Rohan, K. Neufuss, J. Matějíček, J. Dubský, L. Prchlík, C. Holzgartner, (2004), Thermal and mechanical properties of cordierite, mullite and steatite produced by plasma spraying, Ceram. Int. 30:597-603.

[34] H. Schneider, J. Schreuer, B. Hildmann, (2008), Structure and properties of mullite – A review, J. Eur. Ceram. Soc. 28:329-344.

[35] A. Mekap, R.K. Sahoo, A. Das, D. Debasish, S. Bajpai, (2019), Two-step plasma mediated synthesis of mullite and sillimanite powder and their suspensive spray coating on stainless steel, Surf. Coat. Technol. 372:103-110.

[36] K.N. Lee, (2000), Current status of environmental barrier coatings for Si-based ceramics, Surf. Coat. Technol. 133-134:1-7.

[37] S. Dong, J. Zeng, L. Li, J. Sun, X. Yang, H. Liao, (2017), Significance of in-situ dry-ice blasting on the microstructure, crystallinity and bonding strength of plasma-sprayed hydroxyapatite coatings, J. Mech. Bio. Mat. 71:136-147.

[38] S. Dong, B Song, B. Hansz, H. Liao, C. Coddet, (2013), Improvement in the microstructure and property of plasma sprayed metallic, alloy and ceramic coatings by pre-/during treatment of dry-ice blasting, Surf. Coat. Technol. 220:199-203.

[39] M. Vardelle, A. Vardelle, P. Fauchais, (1993), Spray parameters and particle behaviour relationships during plasma spraying, J. Therm. Spray. Technol. 2(1):79-92.

[40] A. Schrijnemakers, B.G. Francq, R. Cloots, B. Vertruyen, F. Boschini, (2013), Mullite plasma spraying for in situ repair of cracks in mullite refractories: simultaneous optimization of porosity and thickness by statistical design of experiments, J. Thermal. Spray. Technol. 22(7):1133-1139.

[41] M.P Planche, J.F. Coudert, P. Fauchais, (1998), Velocity measurements for arc jets produced by a DC plasma spray torch, Plasma Chem. Plasma Process. 18(2):263-283.

[42] G. Hou, X. Zhao, Y. An, H. Zhou, J. Chen, (2018), Effect of spraying parameter and injector angle on the properties of in-flight particles and alumina coatings on Al alloy with PA-HT, Ceram. Int. 44:3173-3182.

[43] S. Kuroda, T.W. Clyne, (1991), The quenching stress in thermally sprayed coatings, Thin solid films 200:49-66.

[44] M. Mutter, G. Mauer, R. Mücke, O. Guillon, R. Vaßen, (2017), Correlation of splat morphologies with porosity and residual stress in plasma-sprayed YSZ coatings, Surf. Coat. Technol. 318:157-169.

[45] M. Mutter, G. Mauer, R. Mücke, R. Vaßen, H.C. Back, J. Gibmeier, (2016), Investigations on the initial stress evolution during atmospheric plasma spraying of YSZ by in situ curvature measurement, J. Thermal. Spray. Technol. 25(4):672-683.

Fig. 1
SEM micrographs of (a), (b) mullite and (c) aromatic polyester powders

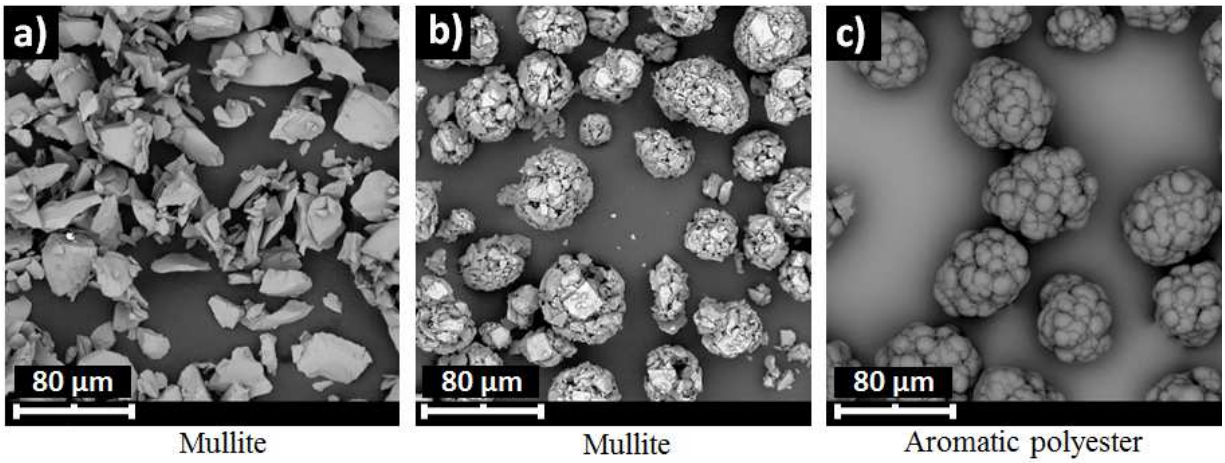

Fig. 2
(a) Schematic illustration of the spray set-up, (b) plasma co-spraying process and identification of relevant deposition parameters

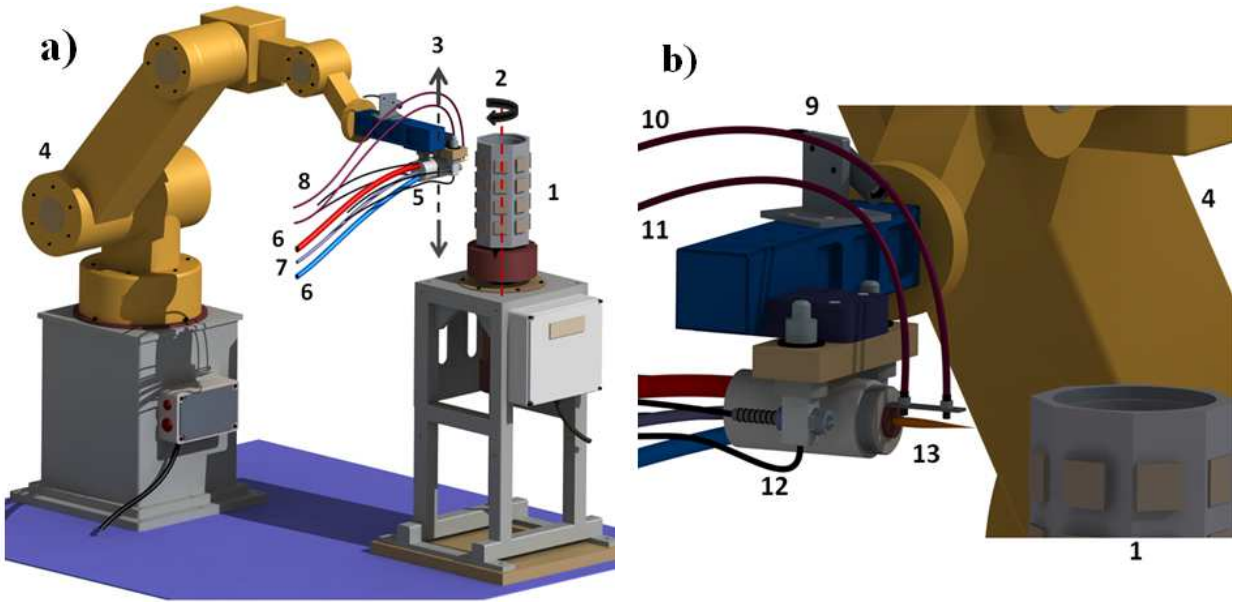

1. Aluminum substrates
2. Cylinder holder rotation direction
3. Torch linear motion
4. 6 - Axis robot
5. Plasma torch
6. Coolant - Power
7. Gases (Ar, H_2, He)
8. Powder feeder pipe
9. Embarked pyrometer
10. Polyester aromatic feeder pipe
11. Mullite feeder pipe
12. Cryogenic cooling system
13. Plasma plume

Fig. 3
SEM images of porous mullite coatings made by plasma co-spraying process, obtained thanks to (a) the organic pore former and (b), (c) mineral pore former. (d), (e) and (f) represent their fracture surface. Microstructures represented in pictures (a), (b), (c) and (f) were obtained with the plasma condition C and fused and crushed powder while the other were obtained with the spray set-up A and the agglomerated and sintered morphology

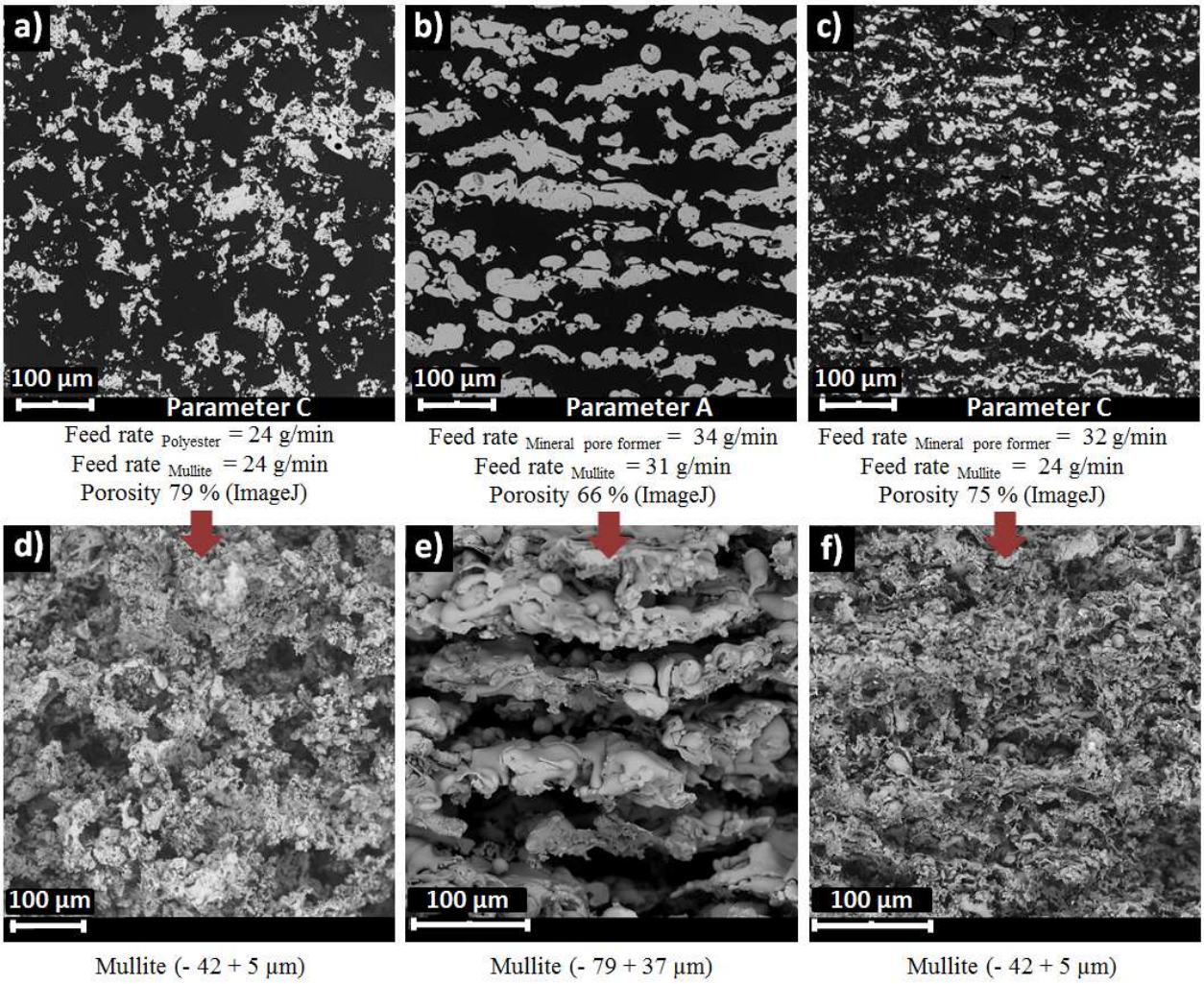

Fig. 4
TGA/DSC results of aromatic polyester powder

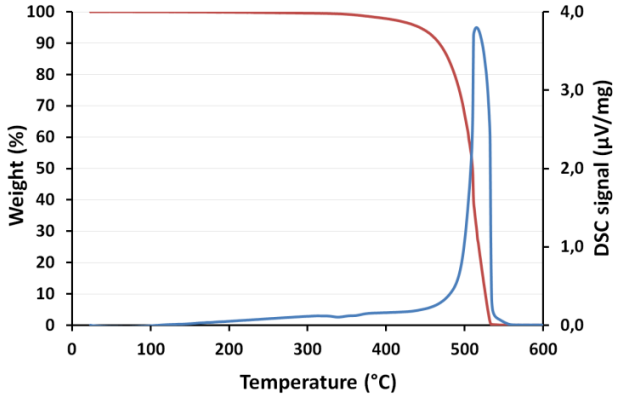

Fig. 5
(a) Porous mullite coating sprayed with the cylindrical configuration, before and after thermal treatment, coating size of 50x50x10 mm, (b) SEM micrograph of porous mullite microstructure obtained on thick coating after thermal treatment, this microstructure is obtained with the fused and crushed powder, spray set-up C and organic pore former

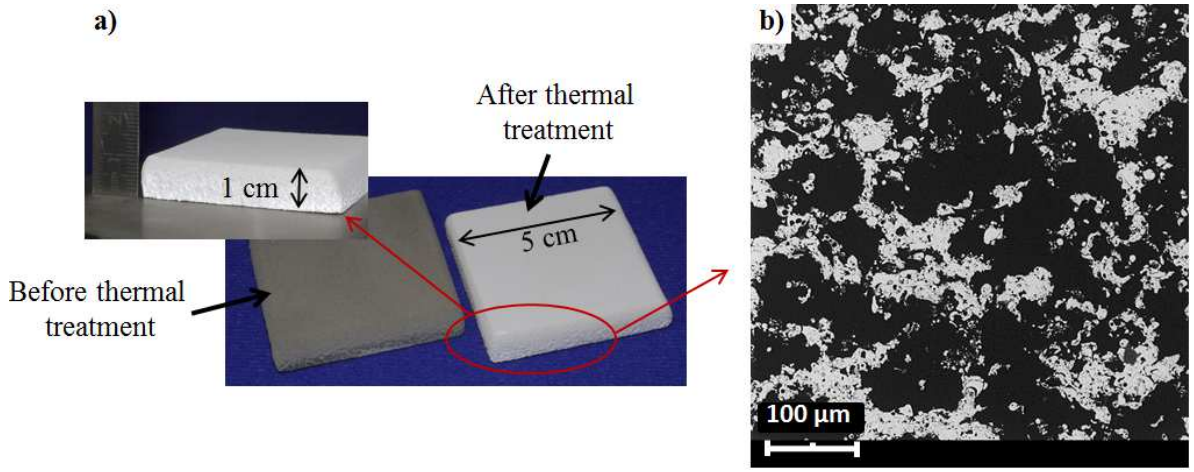

Fig. 6
Schematic illustration of the planar spray set-up

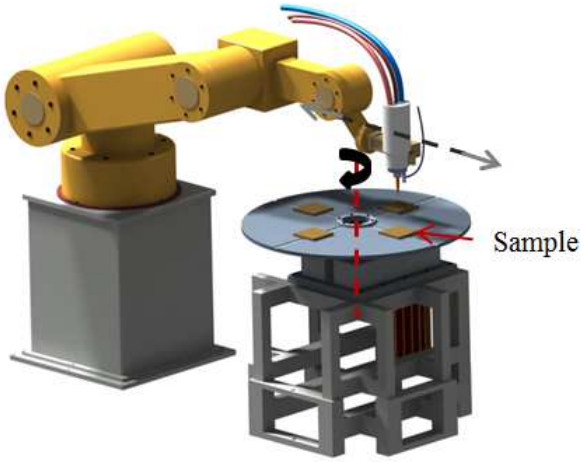

Fig. 7
(a),(b) Free standing mullite/polyester coating sprayed with the planar spray set-up and the mineral bond coat before thermal treatment and (c) after thermal treatment, coating size 100x100x4 mm

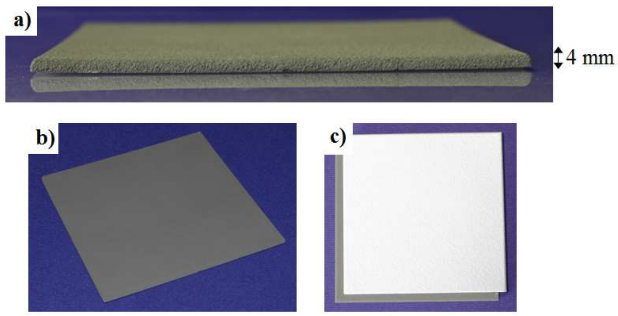

Fig. 8
Approach for getting porous mullite free standing samples with the organic bond coat

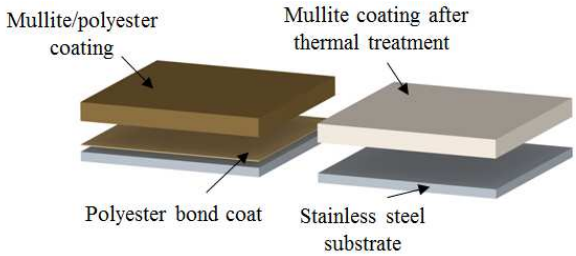

Fig. 9
(a) Sketch of the In-Situ Coating Property (ICP-8) sensor used for the illustration of delamination phenomenon occurring with the planar configuration, (b) mullite/polyester coating sprayed on aluminum substrates with the ICP set-up, with different bond coat natures

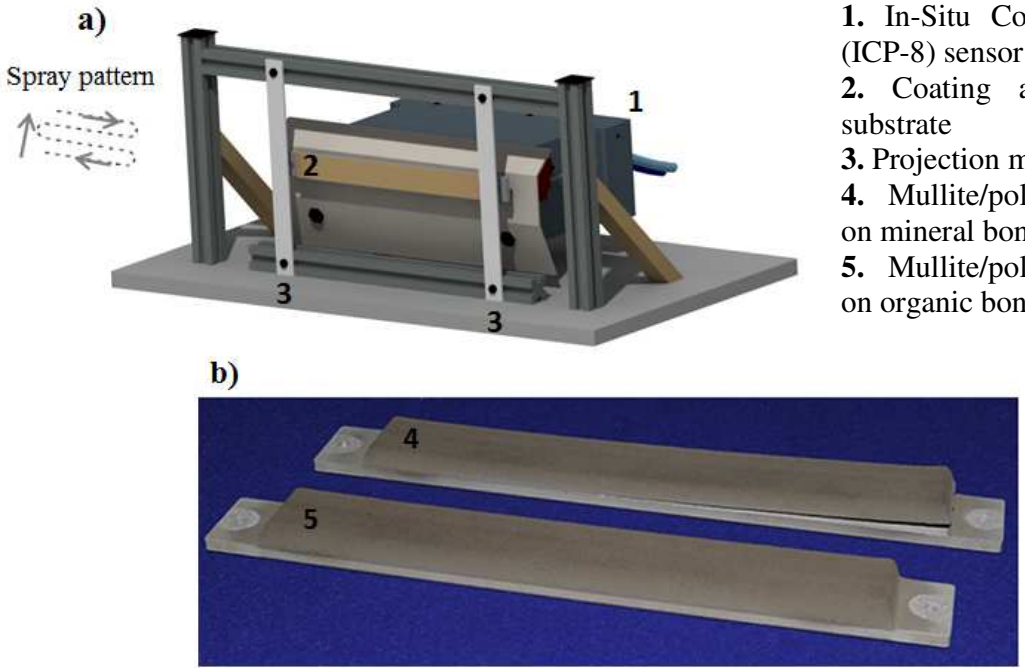

1. In-Situ Coating Property (ICP-8) sensor
2. Coating and aluminum substrate
3. Projection masks
4. Mullite/polyester coating on mineral bond coat
5. Mullite/polyester coating on organic bond coat

Fig. 10
Porous mullite coating sprayed with the planar configuration, (a) before and (b) after thermal treatment, coating size of 100x100x10 mm

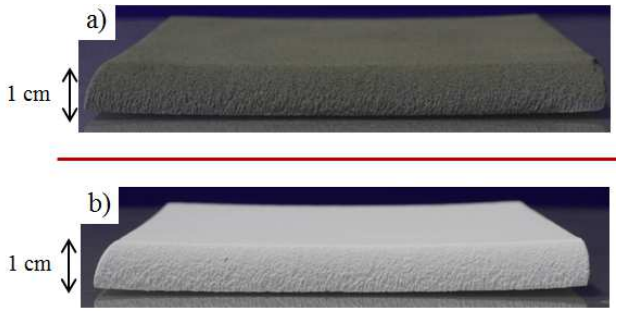

Fig. 11
Schematic illustration of the configuration change, from (a) the planar to (b) static spray set-up

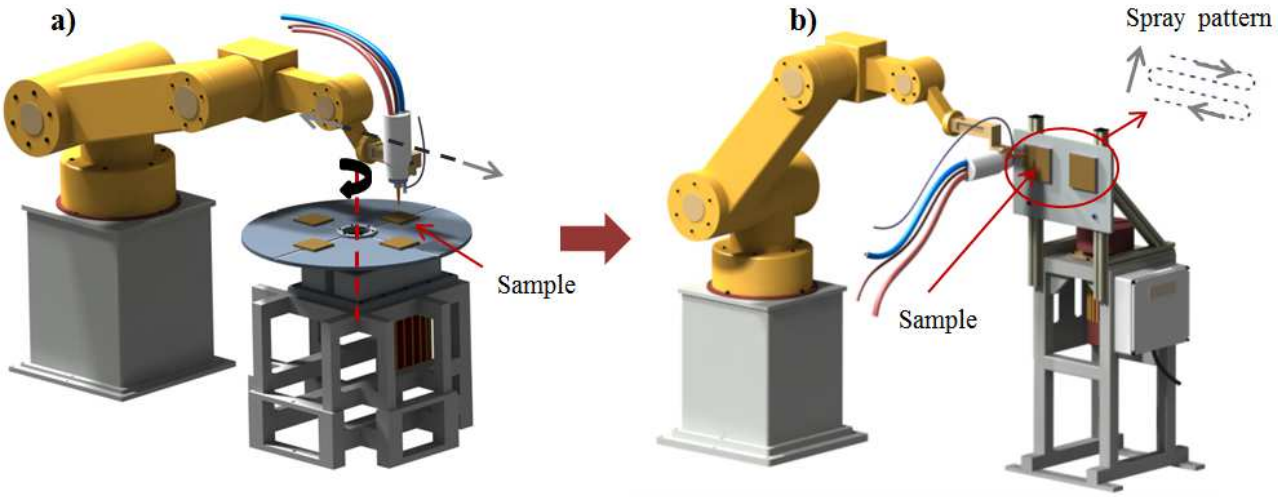

Fig. 12
Comparison between porous mullite coatings sprayed with the (a) planar and (b) static configuration, after thermal treatment, coating size of 100x100x10 mm. Coatings were obtained with the spray set-up C, fused and crushed powder and aromatic polyester as pore former and bond coat

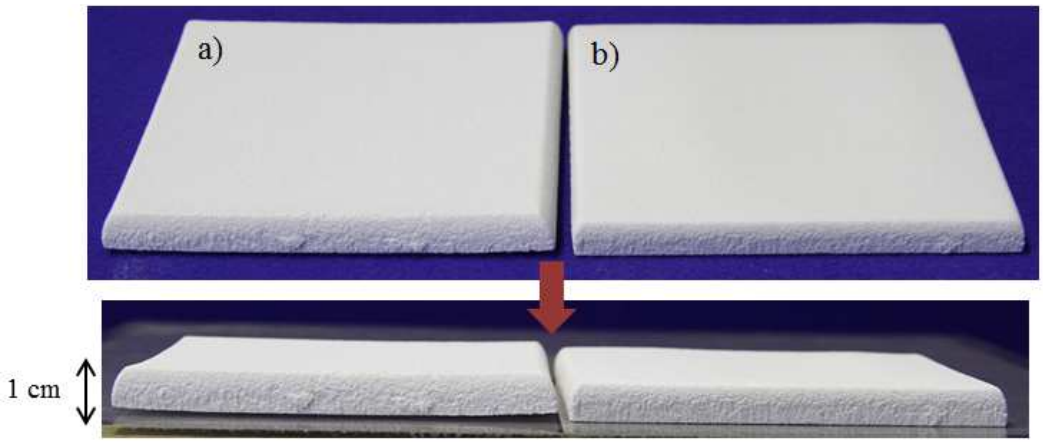

Fig. 13
Evolution of surface temperature depending on the spray set-up: (a) planar, (b) static

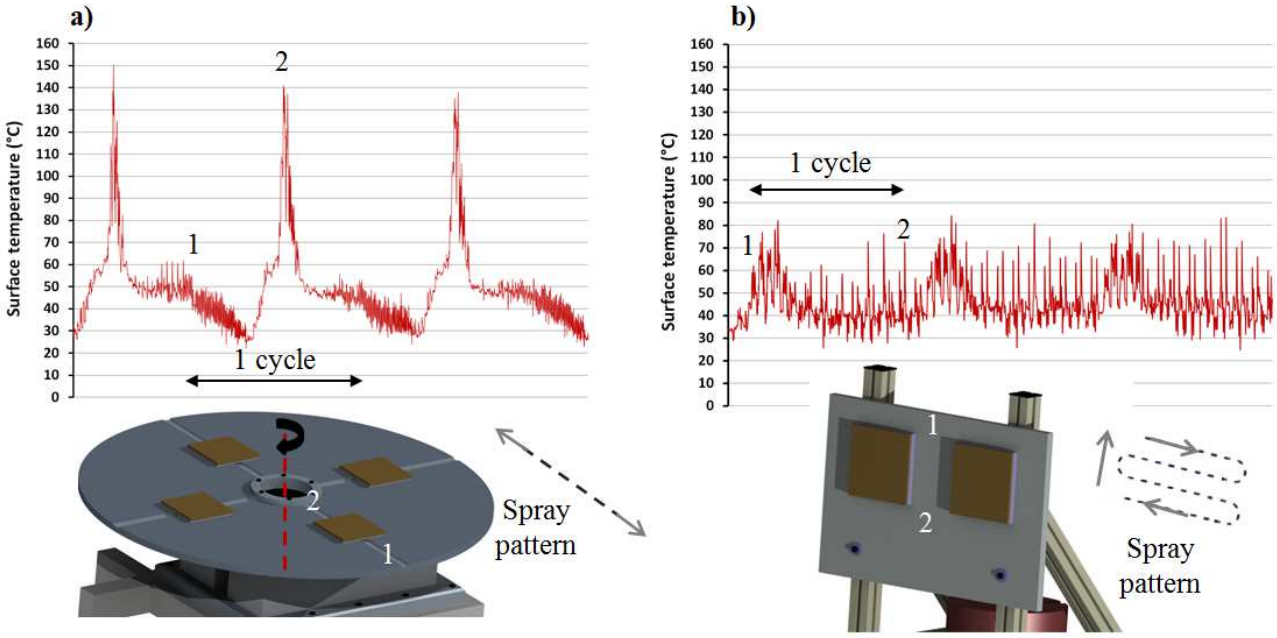

Table 1
Physical properties of mullite

Material	**Mullite**
Density ($g.cm^{-3}$)	2.8 – 3.0
Thermal conductivity ($W.m^{-1}.K^{-1}$)	2.0 – 6.0
Melting point (°C)	1,850
CTE ($10^{-6}.K^{-1}$)	3.5 – 5.0
Specific heat capacity ($J.g^{-1}.K^{-1}$)	0.7 – 1.0
Crystallisation shrinkage (%)	< 1
Crystallisation temperature (°C)	950 – 1,000

Table 2
Plasma spraying parameters with F4-VB torch

Parameters	**A**	**C**
Carrier gaz mixture (%)	29 Ar / 7 H_2 / 64 He	37 Ar / 13 H_2 / 50 He
Intensity (A)	400	600
Electric power (kW)	27	45
Enthalpy ($J.kg^{-1}$)	11	17
Nozzle diameter (mm)	6	6
Standoff distance (mm)	110	110